Simulation of a Mass-Spring-Damper System Using an Analogue Computer

Lukas Kostal

***Abstract*—A theoretical model for an MSD system is described and an analogue op-amp circuit for its real time simulation is presented using parameters characteristic to a standard automotive suspension. The principles of operation of the circuit are discussed along with possible improvements to the design. The experimental setup, used to collect data for various terrain profiles, frequencies and values of ζ is described together with the programs used to analyse the data. The experimental results are then compared with LTspice simulations and solutions obtained by numerical integration. Discrepancies due to steep edges in the terrain profile are discussed. The experimental natural and resonant frequencies are observed to be 12% lower than predicted and this is argued to be caused by the impedance of the oscilloscope probe used to measure the circuits output. The circuits response to varying ζ is shown to agree well with numerical results.**

I. Introduction

Many mechanical systems such as a passive automotive suspension may be reduced to a simple mass-spring-damper model (MSD model) by ignoring any additional structures and assuming a single degree of freedom which is the vertical displacement $y(t)$.

The MSD model behaves as a standard damped harmonic oscillator driven by a contact force from the terrain with a vertical displacement $x(t)$. The response of the system to the terrain is characterised by parameters such as the damping ratio ζ which ultimately determine the driving properties of the vehicle. During development, it is therefore highly desirable to be able to simulate the systems behaviour and observe its response without the need to construct testing prototypes.

An analytical solution can only be found for specific terrain profiles such as a sine wave. For arbitrary terrain profiles the solution can only be found using numerical integration on a digital computer or in real time using op-amps configured as integrating amplifiers in an analogue computer.

II. Theory

Equation (1) is found by resolving forces in the MSD model where $y(t)$ is the systems vertical displacement, m is the mass, b is the damping constant, k is the spring constant and F_x is the driving force exerted on the system.

$$m\ddot{y} + b\dot{y} + ky = F_x \tag{1}$$

Equation (2) is obtained by dividing (1) by m and defining γ and a natural frequency ω_0 as shown below.

$$\gamma = \frac{b}{m} \qquad \omega_0 = \sqrt{\frac{k}{m}} = 2\pi f_0$$

$$\ddot{y} + \gamma\dot{y} + {\omega_0}^2 y = \frac{F_x}{m} \tag{2}$$

By considering the difference $y(t)-x(t)$ between the system and terrain displacements, equation (2) can be rewritten in terms of the terrain displacement $x(t)$, as shown in (3), rather than the force F_x.

$$\ddot{y} + \gamma\left(\dot{y} - \dot{x}\right) + {\omega_0}^2\left(y - x\right) = 0 \tag{3}$$

Additionally a damping ratio ζ can be defined as shown below in (4). For $\zeta < 1$ the system is under-damped, for $\zeta > 1$ over-damped and at $\zeta = 1$ it is critically-damped.

$$\zeta = \frac{b}{2\sqrt{mk}} = \frac{\gamma}{2\omega_0} \tag{4}$$

The parameters of the MSD system to be simulated by the circuit are shown in Tab. I. The peak terrain displacement is chosen to be $0.1\ \mathrm{m}$ representative of an average speed bump.

TABLE I: Physical Parameters

Parameter	Quantity	Units
f_0	1.18	Hz
m	360	kg

Parameters for a standard automobile weighing $1440\ \mathrm{kg}$

III. Theory of Operation

The basic principle behind the operation of the circuit is Kirchhoffs voltage law (KVL). A voltage proportional to the terrain displacement $x(t)$ is applied to the input of the circuit and is gradually processed by op-amp stages into signals which represent the individual terms in (3). The signals are then fed back to be summed creating feedback loops. By KVL the overall potential difference around any of the feedback loops, as well as their sum, will be 0 just like in (3). The signal paths representing the terms $-{\omega_0}^2 x(t)$ and $-\gamma\dot{x}(t)$ are summed without forming a feedback loop, since (3) can be rearranged to have the two terms on the RHS instead of the 0. The output is then taken to be the signal representing $y(t)$.

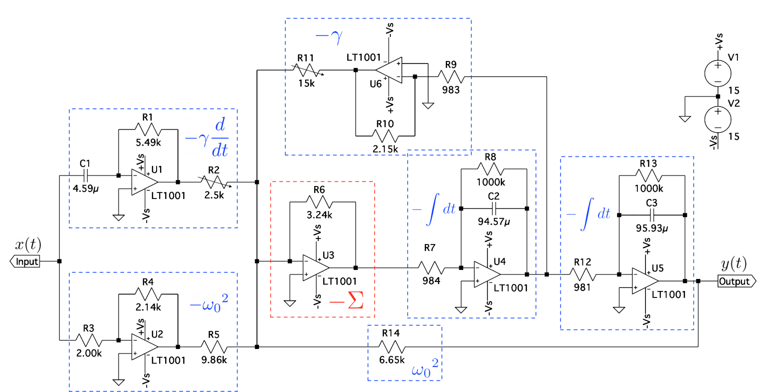

Fig. 1: Circuit schematic of the analogue computer.

The circuit is designed to use the LT1001 precision operational amplifier from Linear Technology [1]. Additionally, the design has been optimised to reduce the total number of op-amps required down to 6.

A. Scaling

If at any stage in the circuit the input voltage to an op-amp exceeds the supply voltage of ± 15 V the op-amp will saturate causing distortions in the final output. Furthermore it is desirable to keep the voltage levels as high as possible, without causing saturation, in order to reduce the effects of noise and maintain a high signal to noise ratio (SNR).

At the input of the circuit this issue is resolved by introducing an external scaling factor s_{ext} in Vm^{-1} which is used to relate the displacement of the driving terrain in m to the input voltage $V_x(t)$ in V as $V_x = s_{ext}x$.

In order to prevent saturation within the circuit, intermediate signals are scaled up and down as required by adjusting the gain of each op-amp stage. This can be done as long as the total gain along a path or around a feedback loop remains equal to the corresponding factor in (3).

Since the output signal $V_y(t)$ is taken from within a feedback loop a uniteless internal scaling factor s_{int} has to be introduced to account for the overall DC gain of the circuit. The scaling factor is given by $s_{int} = \frac{V_y}{V_x}$ and can be used to find the system displacement $y(t)$ in m as $y = \frac{s_{int}}{s_{ext}} V_y$.

B. Varying Zeta

The extent of damping is characterised by ζ which is related to the factor γ as $\gamma = 2{\omega_0}^2\zeta$. In the circuit ζ is varied by varying the resistances R_1 and R_{11} which alter the gain of the signals being summed at U3 as shown in (5) and (7) respectively.

In order to maintain a reasonable signal level the combined gain of U2 and U3 is not exactly ${\omega_0}^2$ but rather involves a scaling factor s_x given by (6). In order to correctly sum the signals the combined gain of U1 and U3 has to account for the factor s_x as shown in. (5).

$$\gamma(R_2) = R_1 C_1 \frac{R_6}{R_2} s_x \tag{5}$$

$$s_x = {\omega_0}^2 \frac{R_3}{R_4} \frac{R_5}{R_6} \tag{6}$$

$$\gamma(R_{11}) = \frac{1}{R_7 C_2} \frac{R_6}{R_{11}} \frac{R_{10}}{R_9} \tag{7}$$

Since the value of ζ has to be the same in both (5) and (7), after substituting the appropriate values, R_2 and R_{11} can be related as $R_{11} \simeq 6R_2$. Values of resistors R2 and R11 must therefore be chosen to satisfy this relationship.

C. Differentiation and Integration

The differentiation of $x(t)$ is performed by an inverting differentiator amplifier stage. In its current implementation the stage is susceptible to noise, due to the capacitor C1 in series with the input, and also suffers from instability resulting in high frequency oscillations with a frequency of $2.18\ \mathrm{kHz}$ at its output. These issues can be resolved by adding a high value resistor in front of C1 and a capacitor in parallel with the feedback resistor R1 which will cause the differentiator amplifier stage to also behave as an active wide band filter.

In the circuit the high frequency oscillations from the differentiator stage are eventually filtered out by the two inverting integrator amplifier stages which act as active low pass filters. The integrator stages also include a $1\ \mathrm{M}\Omega$ resistor in parallel with the feedback capacitor in order to provide DC gain control with a DC gain given by $-\frac{R_8}{R_7}$ [2].

IV. Methodology / Experimental Method

The circuit was constructed on a breadboard according to the schematic shown in Fig. 1. In order to improve the accuracy of the circuit, during construction the resistance values have been measured using an Aim-TTi 1604 bench multimeter [3] and recorded to the nearest 3 significant figures. The capacitor values were also measured using a Digimess RLC 300 LCR meter [4] with an accuracy of $\pm 10\mathrm{nF}$. In order to be able to vary ζ, two resistance decade boxes with a $\pm 1\%$ tolerance were used in place of R2 and R11 as shown in Fig. 2.

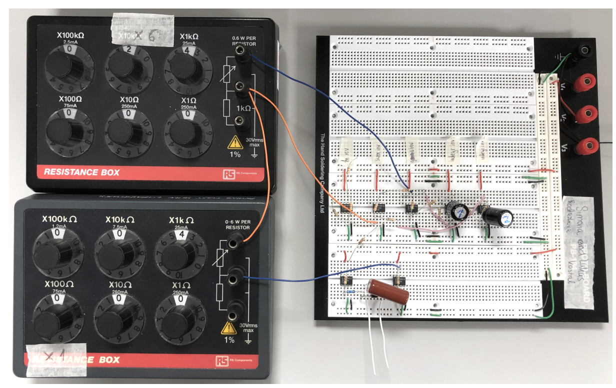

Fig. 2: Photograph of the analogue computer circuit constructed on a breadboard and two resistance decade boxes.

Two Aim-TTi EL302R linear power supplies set to 15 V were used to power the circuit. A Rhode & Schwartz RTB 2004 Oscilloscope [5] was used to both drive the circuit and collect data. The output of the oscilloscopes internal function generator was split using a BNC splitter and connected to the input of the circuit and to Channel 1 on the oscilloscope using standard coaxial cable.

Initially channel 2 on the oscilloscope was connected to the output of the circuit using a simple coaxial cable terminated with two banana plugs. Since the output is obtained from within one of the feedback loops the large capacitance of the coaxial cable [6] has resulted in high frequency (HF) oscillations within the circuit. To resolve the issue the coaxial cable has been replaced by a passive 1:1 oscilloscope probe.

The oscilloscope was then set into roll mode with DC coupling and HF reject set on both channels. The function generator output was switched on and the measured waveforms were saved in the form of .csv files along with screenshots.

The decade boxes were set to $R_2 = 2.5$ kΩ and $R_{11} = 15$ kΩ and a set of 3 measurements at driving frequencies $f = 0.2, 0.5, 1.2$ Hz was taken for each of the waveforms shown in Tab. II. A half rectified sine wave was obtained by connecting a 1N4007 rectifier diode in series with the input.

TABLE II: Tested Waveforms

Waveform	Peak to Peak Voltage / V	DC offset / V
Square	4.00	2.00
Triangle	4.00	2.00
Sine	5.00	0
Sine (before half rectification)	5.00	1.00

Waveforms used to test the performance of the circuit.

Without adjusting the decade boxes, a set of 25 measurements was taken to analyse the frequency response of the circuit using a 5 V peak to peak sine wave with frequencies varying from 0.1 Hz to 2.5 Hz in increments of 0.1 Hz.

To analyse the circuits response to varying ζ, a set of 14 measurements was taken for the square wave shown in Tab. II at a frequency of 0.1 Hz, while varying the decade boxes from $R_2 = 0.7$ kΩ up to $R_2 = 4.6$ kΩ in increments of 0.3 kΩ and maintaining the relationship $R_{11} \simeq 6R_2$.

V. Data Analysis

LTspice [7] is used to produce simulated waveforms corresponding to the obtained experimental waveforms. The experimental and simulated waveforms are then analysed using 3 analysis programs written in Python.

The program processes the waveforms and generates a waveform representing an exact numerical solution to (3). This is accomplished by using the measured input waveform to calculate values of $x(t)$ which are then fed into (3) while it is solved using the scipy.integrate.solve_ivp function from the SciPy library [8]. This process is accelerated using the Numba JIT compiler library [9].

The exact functioning of the programs is described in the code which can be found on the projects GitHub repository [10] along with the raw experimental data, LTspice simulations, photographs of the experimental setup and additional results.

VI. Results and Discussion

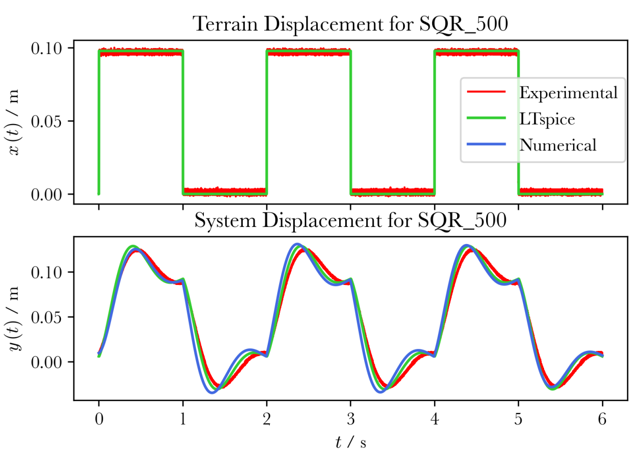

Fig. 3: Square terrain profile, $f = 0.5$ Hz, $\zeta = 0.343$ kgs^{-1}.

As can be seen from Fig. 3 the peaks in $y(t)$ which are a response to the edges in the square wave $x(t)$ appear lower and less sharp on the experimental waveform compared to the numerical waveform. This occurs mainly because any rapidly changing signals on the circuits input result in large spikes at the output of the differentiator stage. For a square wave the spikes lead to a saturation of U3 for approximately 50ms.

This in combination with a finite slew rate of the op-amps and the previously discussed instability of the differentiator results in the observed discrepancy.

The saturation could be resolved by scaling the signal down however, this would decrease the signal to noise ratio and for any theoretically discontinuous function such as the square wave a momentary saturation is inevitable.

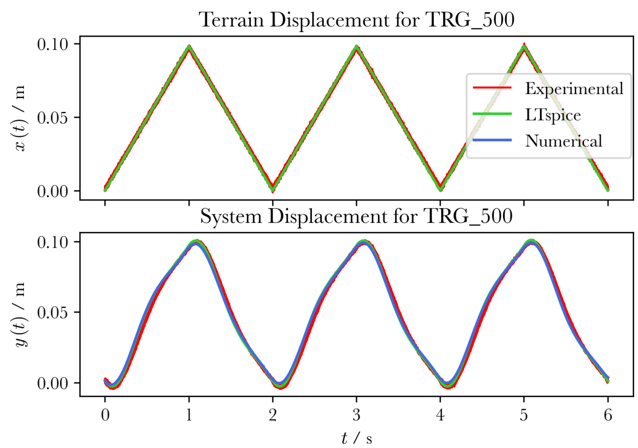

Fig. 4: Triangular terrain profile, $f = 0.5$ Hz, $\zeta = 0.343$ kgs^{-1}.

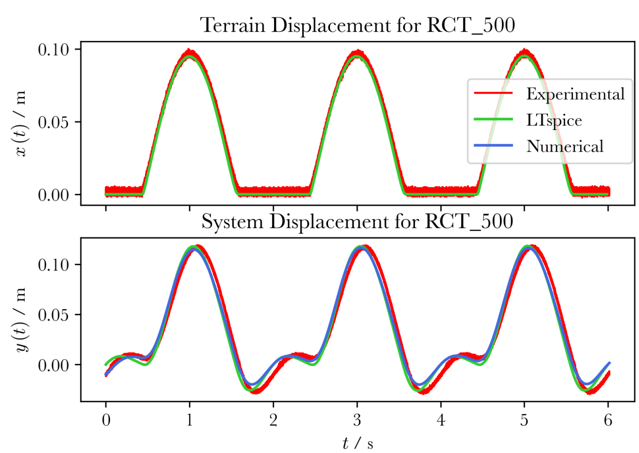

Fig. 5: Half rectified sine wave terrain profile, $f = 0.5$ Hz, $\zeta = 0.343$ kgs^{-1}.

Fig. 4 and Fig. 5 show that for triangular and sinusoidal terrain profiles the experimental waveforms agree with the numerical solutions. The only discrepancy, due to the same reasons as in Fig. 3, can be seen on Fig. 5 in the sudden transition from a sine wave to a horizontal terrain.

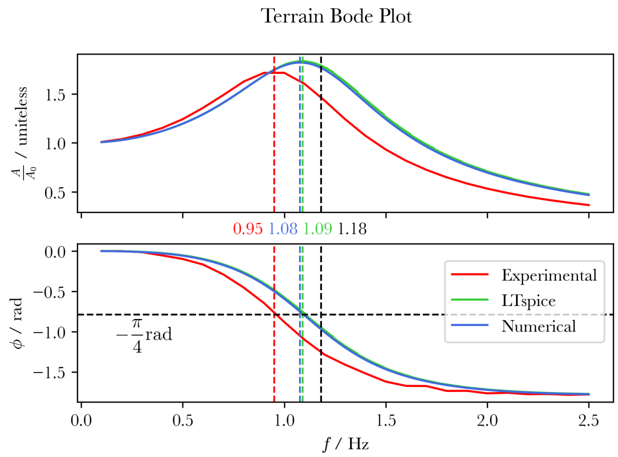

Fig. 6: Bode plot for a 0.1 m sinusoidal terrain profile, $\zeta = 0.343$ kgs^{-1}.

For an MSD system the resonant frequency f_{res} is slightly lower than the natural frequency f_0 and they are related as shown by (8). This relation is slightly different than the usual $f_{res} = f_0\sqrt{1-2\,\zeta^2}$ since (3) is written in terms of the displacement $x(t)$ rather than the force F_x.

$$2\zeta^2 {f_{res}}^4 + {f_0}^2 {f_{res}}^3 - {f_0}^2 = 0 \tag{8}$$

As shown on Fig. 6 the experimental resonant frequency is lower than the numerical resonant frequency with a percentage difference of 12%. This can also be seen in Fig. 7 where after being displaced the experimental waveform oscillates at a lower natural frequency than the other two waveforms.

It can also be seen that the experimental and numerical amplitudes agree well for frequencies below 1.00 Hz after which the experimental amplitude starts to decrease.

The discrepancy in amplitude and f_{res} must be due to external effects since it only appears on the experimental curve and not the LTspice simulation. It can therefore be concluded that it is caused by the impedance of the oscilloscope probe used to make the measurement. Since the probe is connected to a feedback loop responsible for the factor ${\omega_0}^2$ it interferes with the feedback and decreases the overall loop gain causing a lower ω_0 and f_{res}. The issue should be reduced by using a high impedance probe such as a 10:1 passive probe.

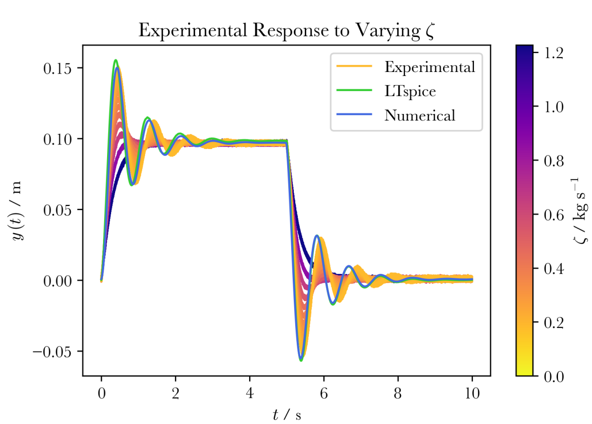

Fig. 7: Color map plot for a 0.1 m square terrain profile showing the effect of varying ζ at $f = 0.1$ Hz.

Fig. 7 shows the response of the circuit to be stable even at light damping given by high values of R_2 and R_{11}.

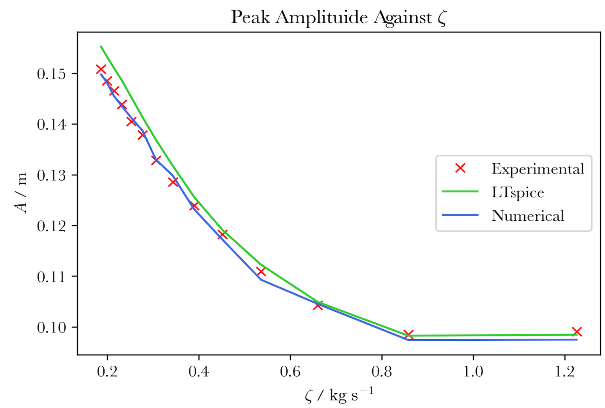

Fig. 8: Plot of peak amplitude A from Fig. 7 against ζ.

From Fig. 8 it can be seen that the peaks of the experimental and numerical waveforms agree to within 2 mm over the entire range of ζ tested ranging from light damping at $\zeta = 0.187$ kgs^{-1} to heavy damping at $\zeta = 1.23$ kgs^{-1}.

VII. Conclusion

Causes of issues within the presented circuit design such as momentary saturation, noise and instability have been discussed along with possible solutions. Comparison of experimental data with LTspice simulations and numerical solutions for the MSD system have shown the saturation and instability issues to be of little significance, however a bode plot has revealed the experimental resonant and natural frequencies to be 12% lower than those for the numerical solution and LTspice simulation. This was then shown to be caused by the impedance of the oscilloscope probe used to measure the circuits output. An analysis of the circuits response to varying zeta has shown the circuits output to be in good agreement with the numerical solution for a wide range of values of ζ. It can therefore be concluded that the proposed circuit is capable of accurate real time simulation of an MSD system for an arbitrary terrain profile.

In addition to the performed analysis the collected data could also be used to produce FFT power spectra and FFT spectrograms for analysis of high frequency resonance in the input and output signals. Although preferably for this, new data should be collected using a spectrum analyser.

A valuable but lengthy additional experiment would be to analyse the circuits frequency response, such as the one shown in Fig. 6, over a range of values of ζ. The data could then be used to observe the effects of varying ζ on the shape of the resonance curve.

Other remaining experiments which could help characterise the circuits properties include an electro magnetic noise susceptibility analysis, temperature stability analysis and long term performance evaluation.

REFERENCES

[1] *LT1001 Precision Amplifier Datasheet*, Analog Devices Inc., Massachusetts, United States. [Online]. Available: https://www.analog.com/media/en/technical-documentation/data-sheets/LT1001.pdf

[2] P. Tapashetti, A. Gupta, C. Mithlesh, and A. Umesh, "Design and simulation of op amp integrator and its applications," *International Journal of Engineering and Advanced Technology (IJEAT)*, vol. 1, no. 3, pp. 12–19, 2012.

[3] *Model 1604 Multimeter Datasheet*, Cambridgeshire, United Kingdom. [Online]. Available: https://resources.aimtti.com/datasheetAIM-1604_multimeter_data_sheet-Iss2A.pdf

[4] *RLC 300 Automatic RLC Meter Datasheet*, Derby, United Kingdom. [Online]. Available: http://www.digimessinstruments.co.uk/datasheets/english/drlc300eng.pdf

[5] *RTB2000 Oscilloscope Datasheet*, Rohde and Schwarz GmbH & Co. KG, Munich, Germany, 2019.

[6] A. C. Melissinos and J. Napolitano, *Experiments in Modern Physics*. Gulf Professional Publishing, 2003.

[7] Analog Devices, Inc., "Ltspice," 2022. [Online]. Available: https://www.analog.com/en/design-center/design-tools-and-calculators/ltspice-simulator.html

[8] P. Virtanen, R. Gommers, T. E. Oliphant, M. Haberland, T. Reddy, D. Cournapeau, E. Burovski, P. Peterson, W. Weckesser, J. Bright, S. J. van der Walt, M. Brett, J. Wilson, K. J. Millman, N. Mayorov, A. R. J. Nelson, E. Jones, R. Kern, E. Larson, C. J. Carey, İ. Polat, Y. Feng, E. W. Moore, J. VanderPlas, D. Laxalde, J. Perktold, R. Cimrman, I. Henriksen, E. A. Quintero, C. R. Harris, A. M. Archibald, A. H. Ribeiro, F. Pedregosa, P. van Mulbregt, and SciPy 1.0 Contributors, "SciPy 1.0: Fundamental Algorithms for Scientific Computing in Python," *Nature Methods*, vol. 17, pp. 261–272, 2020.

[9] S. K. Lam, A. Pitrou, and S. Seibert, "Numba: A llvm-based python jit compiler," in *Proceedings of the Second Workshop on the LLVM Compiler Infrastructure in HPC*, 2015, pp. 1–6.

[10] L. Kostal, "Simulation of mass-spring-damper system using an analogue computer github repository," 2022. [Online]. Available: https://github.com/KostalLukas/Simulation-of-Mass-Spring-Damper-System-Using-an-Analogue-Computer